Transition metal complexes as the potential tools against SARS-CoV-2: *In silico* approach

*Maynak Pal, Dulal Musib and Mithun Roy**

Supporting Information

Table of Content

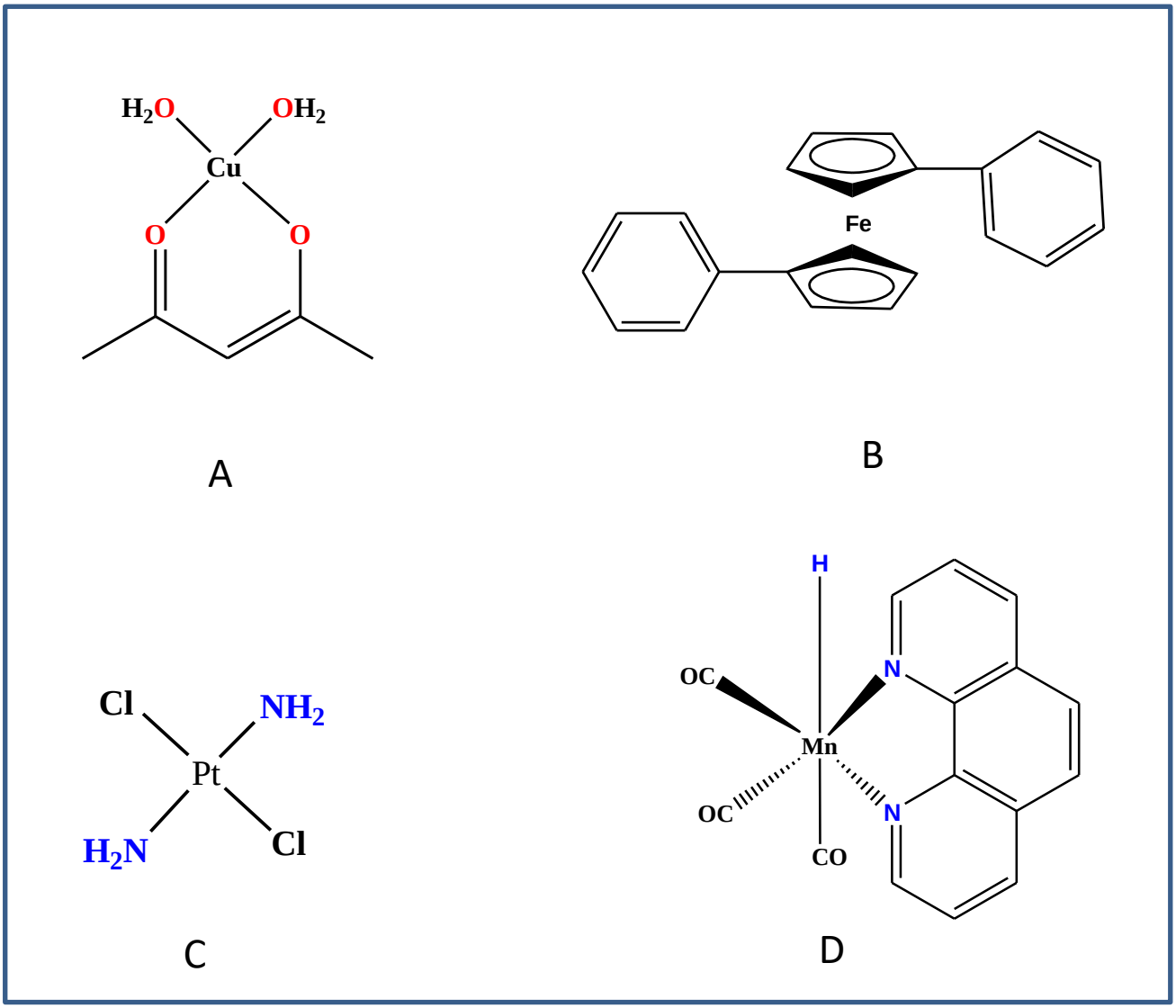

Scheme S1 : Control complexes for understanding the structure activity relationship for molecular docking of metal complexes in the RdRp of SARS-CoV-2.

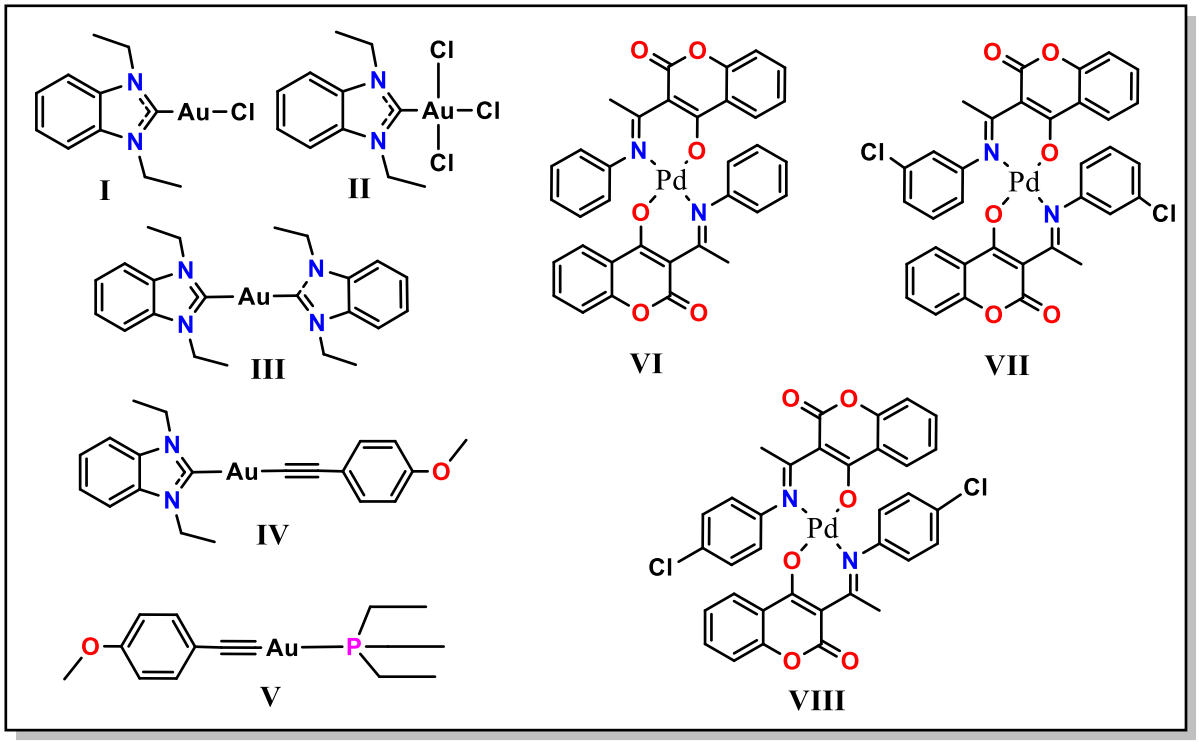

Scheme S2 : Literature reports of metal complexes used as SARS-CoV-2 inhibitor[1-2].

Table S1 : The percentage of structural similarity of different virus (e.g HIV, HCD, etc.) vs SARS-CoV-2.

PDB ID (SARS-CoV-2 Target Protein, RdRp)	PDB ID (Target Protein of different Virues)	Similarity percentage (%)
6M71	2WGU (Ads)	58.76
6M71	4TVG (HIV)	71.72
6M71	2GV9 (HSV)	60.23
6M71	4N0Y (HCV)	75.32
6M71	5V13 (mJHBP)	58.68
6M71	4M9F (Dengue)	55.47

Table S2: The probable interaction between the complexes and their reported target proteins determined from molecular docking studies

Complex	Protein PDB ID	Binding Energy	Inhibition constant (μM)	Inter-molecular energy	vdw HB Desolvation energy	Electrostatic energy	Total internal energy	Torsional energy
1	2WGU	-8.22	0.944	-8.52	-8.41	-0.11	19.0	0.3
2	4TVG	-6.69	12.49	-9.37	-9.19	-0.19	7.6	2.68
3	4TVG	-7.37	3.98	-13.63	-13.72	0.09	3.62	6.26
4	2GV9	-7.25	4.84	-10.53	-9.85	-0.68	-3.3	3.28
5	4N0Y	-7.46	3.42	-8.95	-9.08	0.13	-1.59	1.49
6	4N0Y	-9.35	0.139	-12.93	-12.43	-0.5	-5.5	3.58
7	5V13	-7.51	3.14	-8.4	-8.44	0.04	-0.71	0.89
8	5V13	-7.43	3.58	-8.92	-8.77	-0.15	-1.36	1.49
9	3OE6	-9.19	0.183	-10.38	-10.41	0.03	-0.75	1.19
10	4M9F	-8.17	1.03	-9.36	-9.18	-0.18	-0.89	1.19
11	4M9F	-8.19	0.999	-8.78	-8.36	-0.42	-0.44	0.6
Curcumin	6M71	-6.47	17.96	-9.46	-9.37	-0.09	-2.29	2.98
Quine	6M71	-8.5	0.585	-9.7	-9.69	-0.01	-2.25	1.19
A	6M71	-4.92	245.92	-5.52	-5.51	-0.01	-0.3	0.6
B	6M71	-5.95	43.53	-7.74	-7.74	0	-1.01	1.79
C	6M71	-6.05	36.85	-6.05	-6.09	0.05	0	0
D	6M71	-4.37	624.12	-4.97	-4.94	-0.03	-0.13	0.6

The table above depicts the details of the interactions between the RdRp of SARS-CoV-2 and the complexes, The energy values are given in the unit of Kcal/mol. The binding energy is corresponding to the binding free energy (ΔG) between the complex and RdRp. All other factors directly attributes to the binding energy. The molecular docking is performed on the protrein with PDB ID 6M71. The grid center at 103.434, 97.322, 112.467 (x,y,z coordinate) and grid size of 126 X 80 X 100 (x X y X z) with spacing 0.375 Å. The docking calculations were carried out by general algorithm parameters with 10 runs of population size 150. The maximum number of evaluations was set to be 25000000 (long) with the rate of gene mutation 0.02 and the rate of crossover mode 0.8.

Table S3 : Litarature report of the active metal complexes against SARS-CoV-2.

Compound Name	spike-ACE2 (IC_{50}, µM)	PLpro (IC_{50}, µM)	Reference
I	22.2±2.8	25.5±1.2	1
II	19.4±5.7	6.3±1.6	1
III	21.3±6.8	14.2±0.3	1
IV	25.0±4.2	14.1±2.1	1
V	16.2±2.4	6.7±0.9	1
VI	-	17.94 (nM)	2
VII	-	2.33 (nM)	2
VIII	-	7.55 (nM)	2

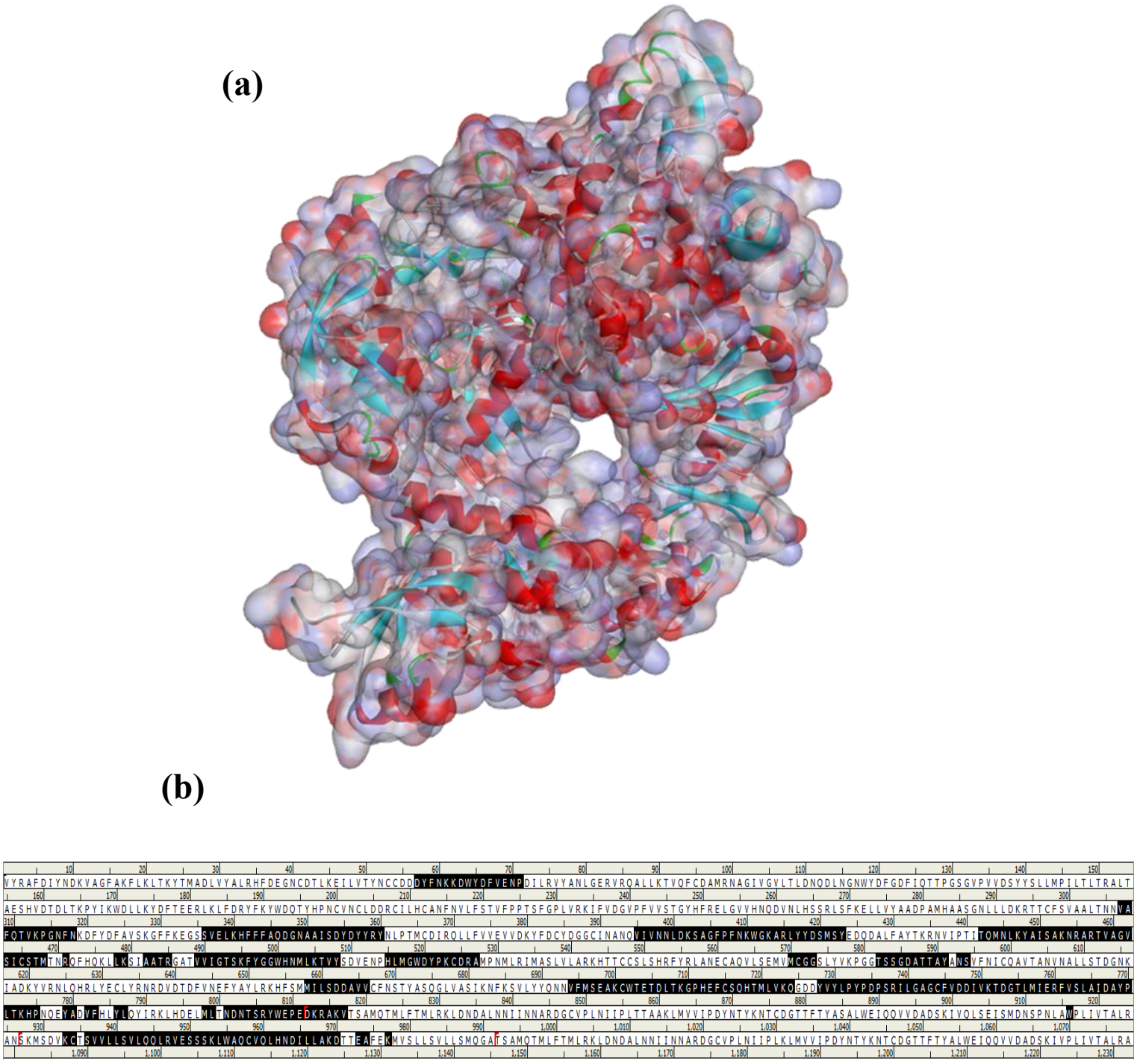

Figure S1. (a) The binding pocket of RdRp complex of SARS-CoV-2; (b) Details protein sequence of the RdRp protein of SARS-CoV-2, the residue of binding pocket is highlighted in black.

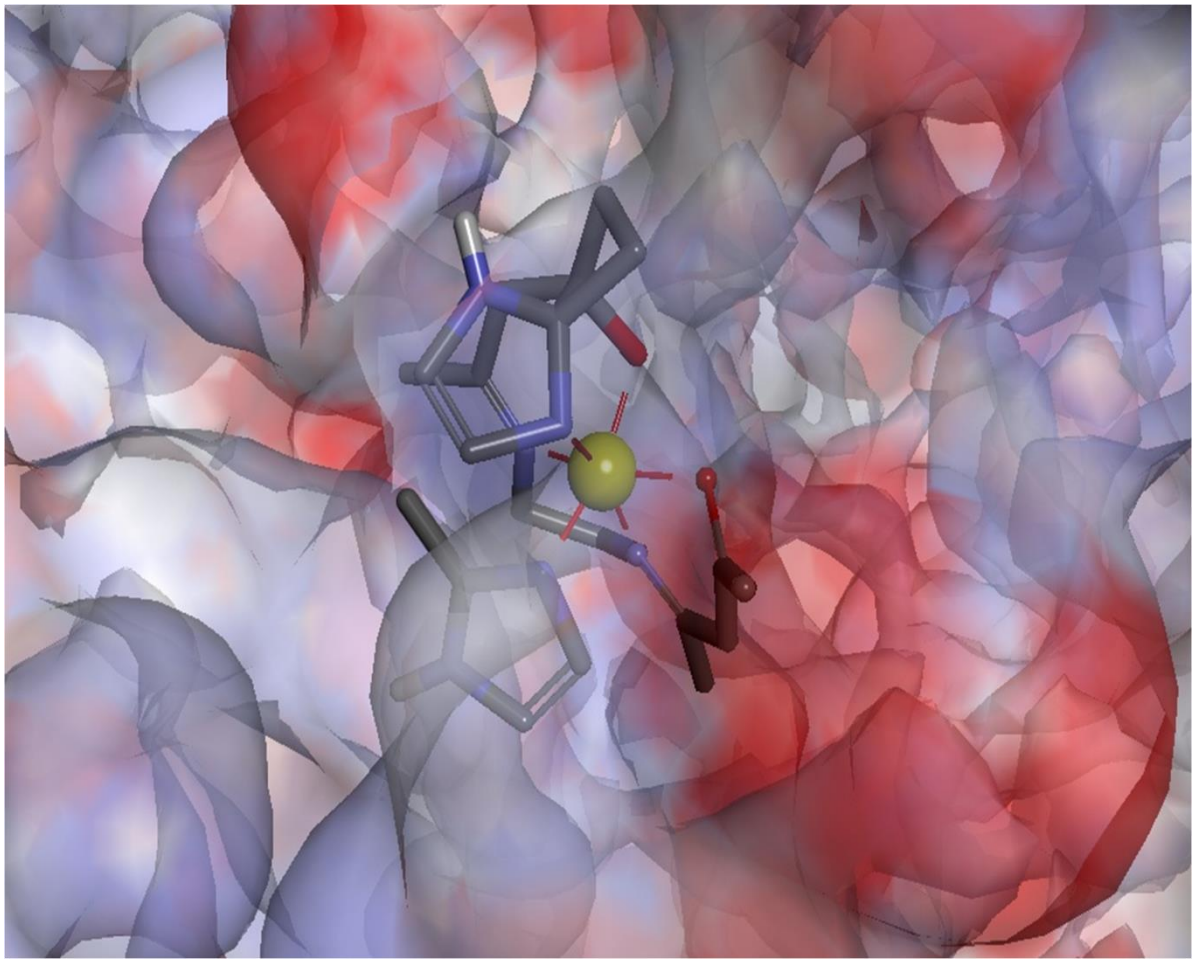

Figure S2. Docked pose of complex 1 in the RdRp complex of SARS-CoV-2.

(a) **(b)**

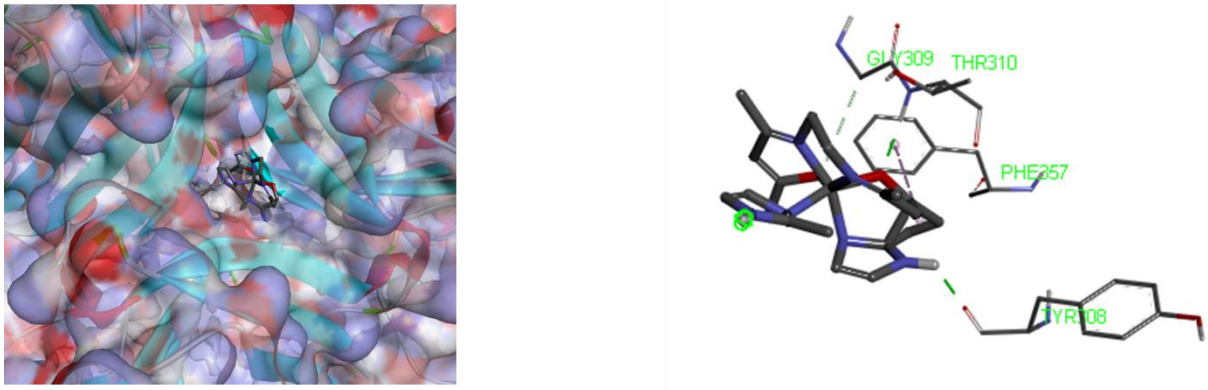

Figure S3. (a) Docked pose of complex 1 in the 2WGU protein of Human Adenovirus; (b) Hydrogen bonding and alkyl-π interaction with the complex and THR310, TYR308, PHE357 residue of the protein and the complex.

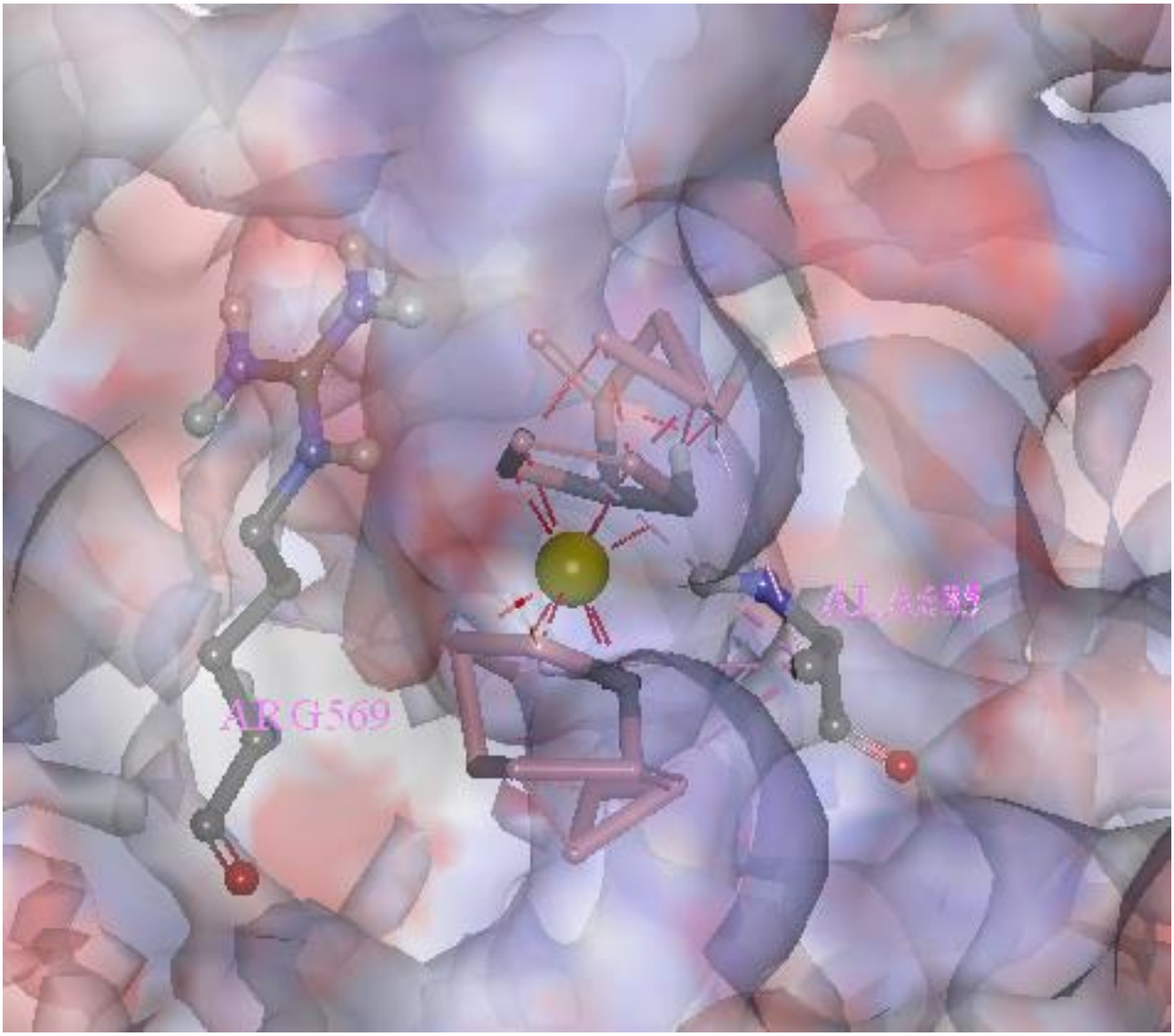

Figure S4. Docked pose of complex 2 in the RdRp complex of SARS-CoV-2.

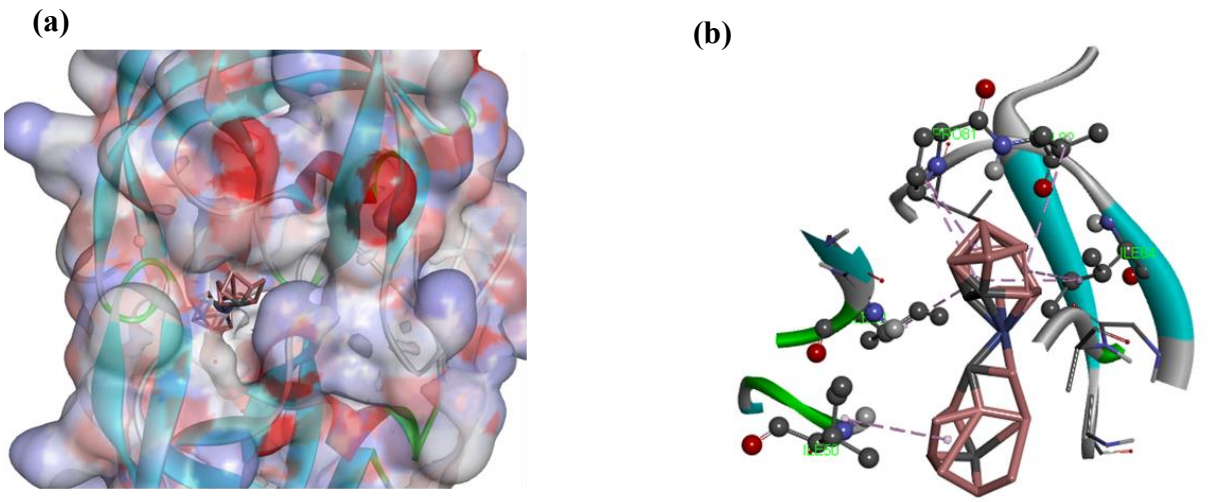

Figure S5. (a) Docked pose of complex 2 in the 4TVG protein of HIV-protease; (b) The alkyl-π interactions with the PRO81, ILE84, ILE50, VAL82 residue, coordinate covalent interaction with the ILE 50 of the protein 4TVG and the complex.

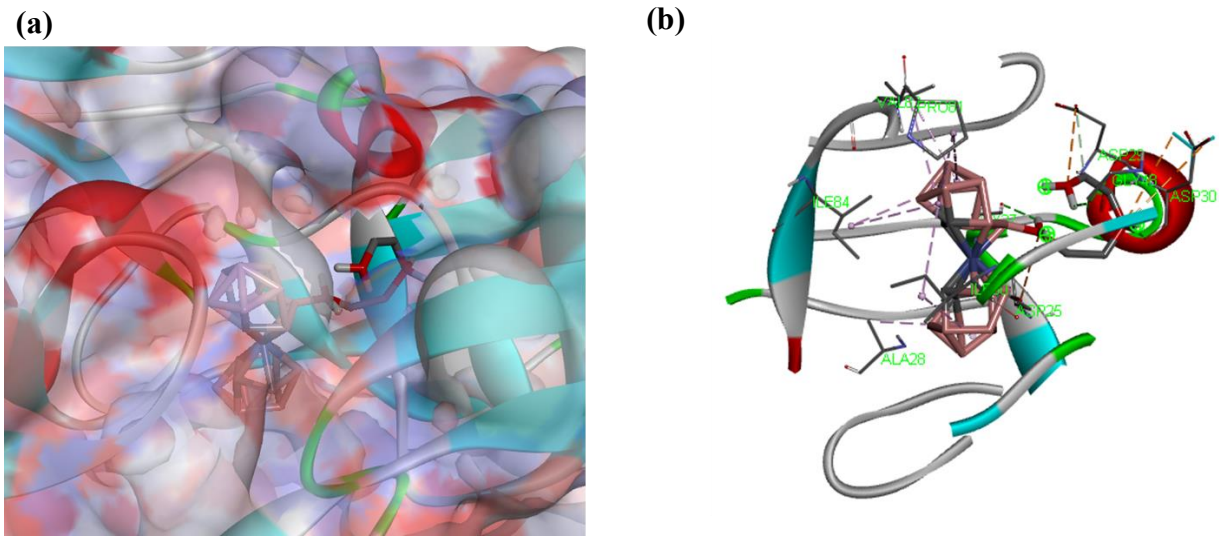

Figure S6. (a) Docked pose of complex 3 in the 4TVG protein of HIV-protease; (b) The non covalent interaction with VAL82, PRO81, ILE84, ILE50, ALA28 residue of the protein and the complex.

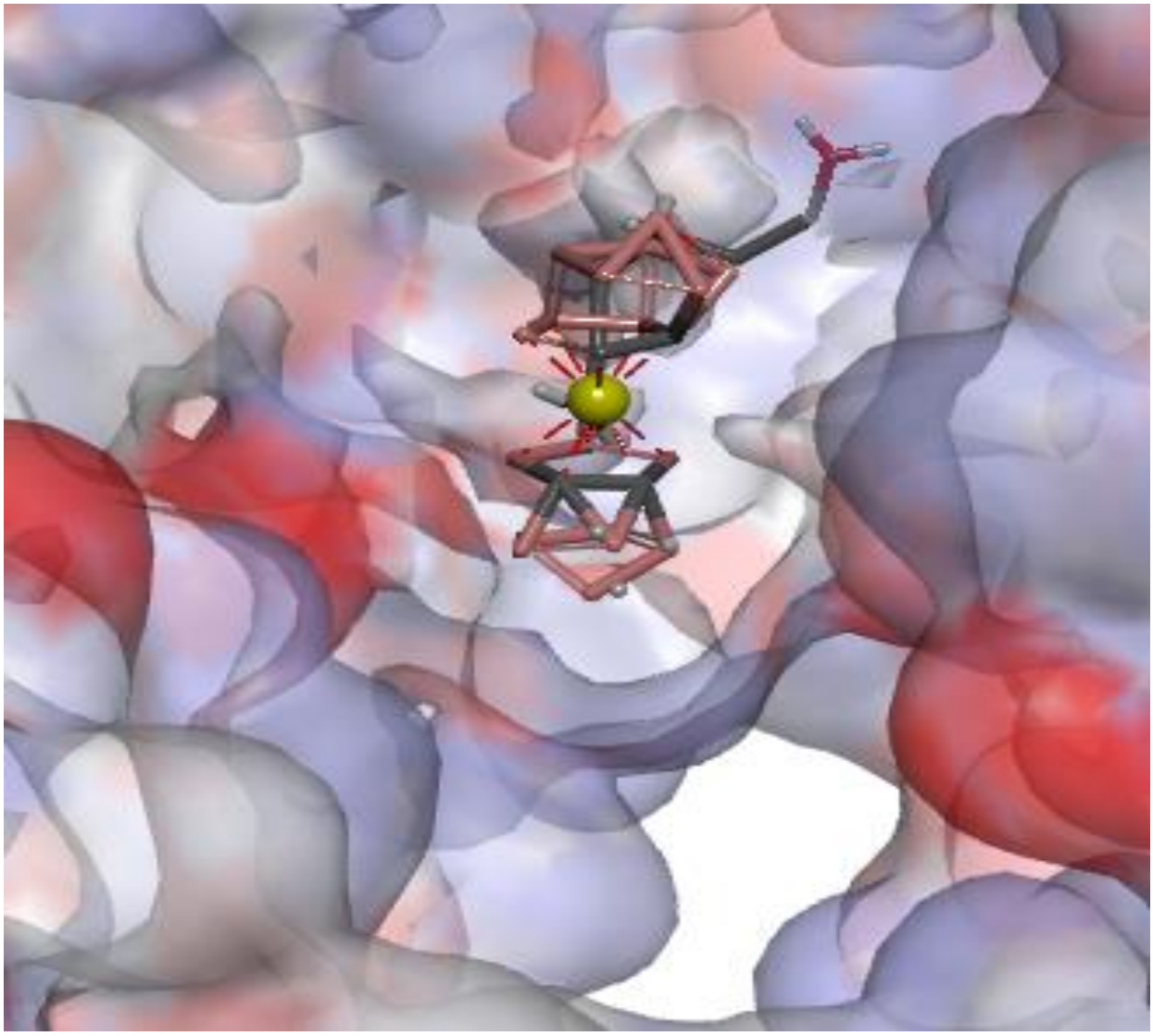

Figure S7. Docked pose of complex 3 in the RdRp complex of SARS-CoV-2.

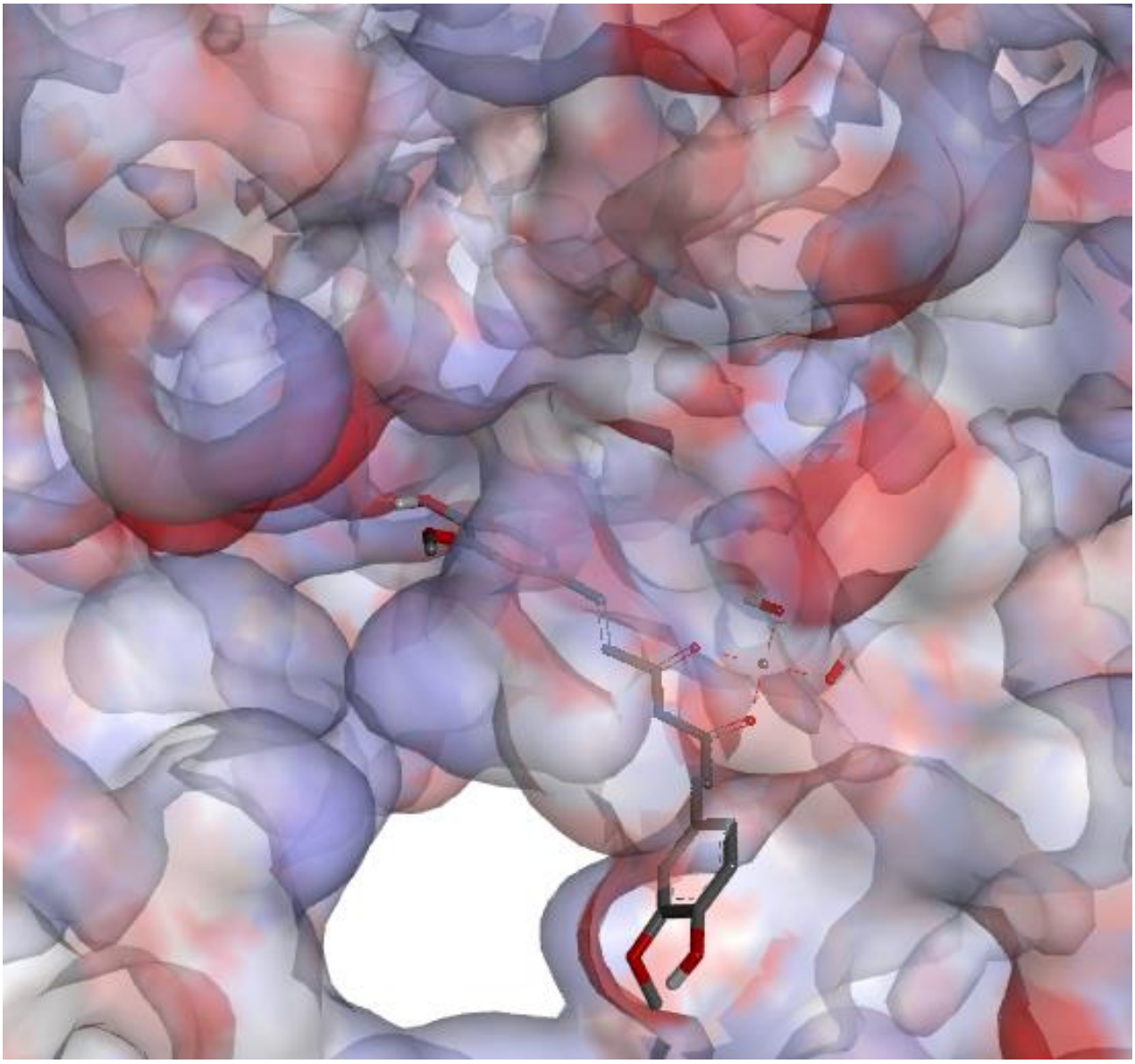

Figure S8. Docked pose of complex 4 in the RdRp complex of SARS-CoV-2.

(a) **(b)**

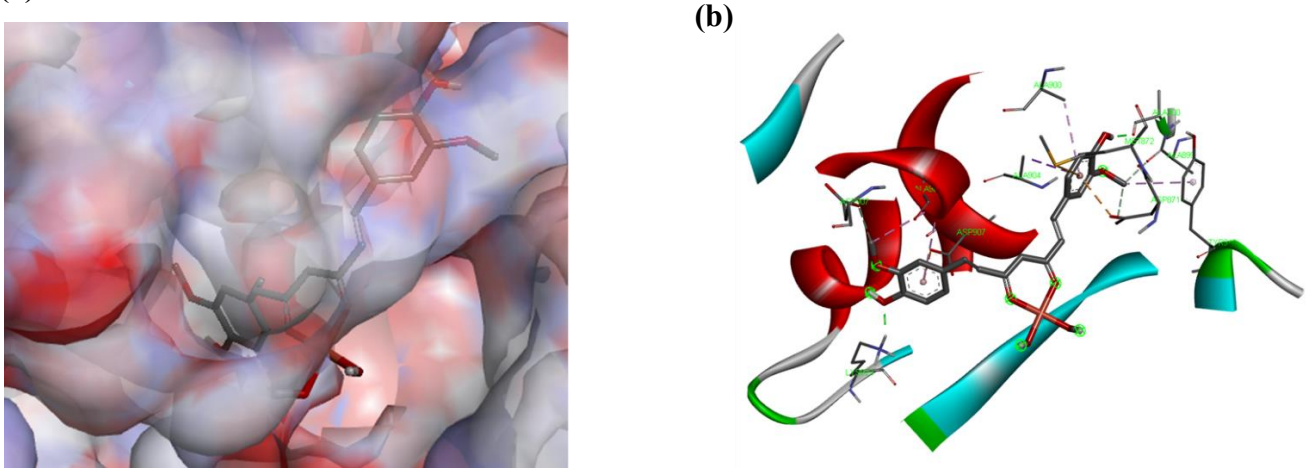

Figure S9. (a) Docked pose of complex 4 in the 2VG9 protein of HSV-1 virus; (b) Hydrogen bonding interaction with the ALA900 and LYS923 residue, alkyl-π interactions with the TYR946 and ALA904 residue, π-σ inteactions of the ALA904 residue of the protein 2VG9 and the complex.

(a) **(b)**

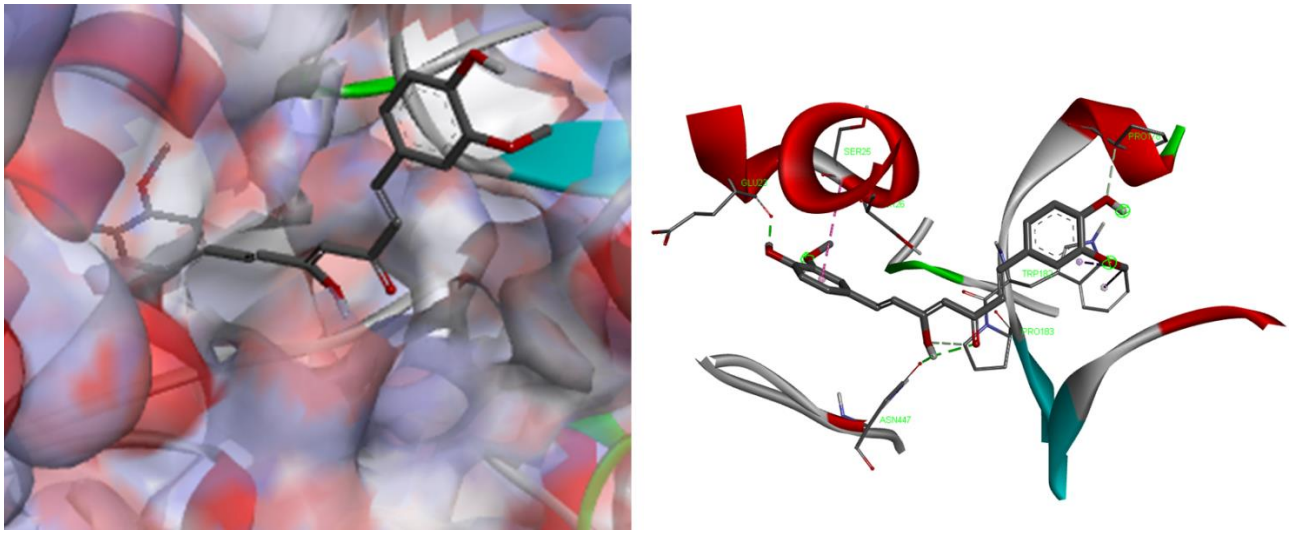

Figure S10. (a) Docked pose of curcumin in the RdRp of SARS-CoV-2; (b) Hydogen bonding interaction with the ASN447 residue and GLU23 residue of the protein and the curcumin.

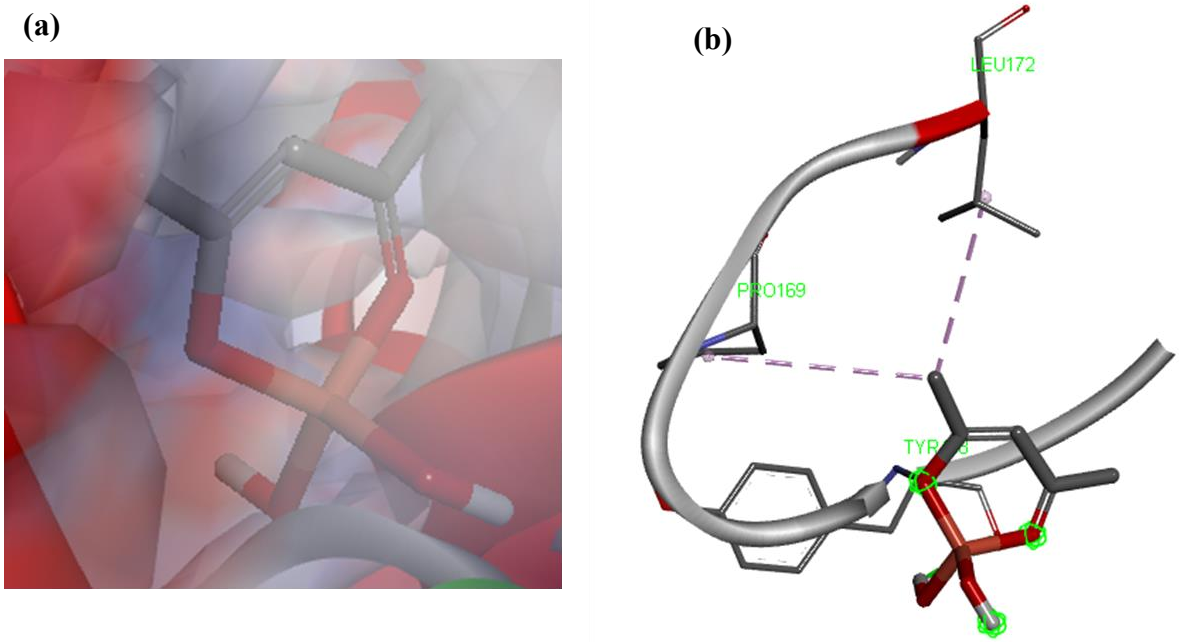

Figure S11. (a) Docked pose of control complex A in the RdRp of SARS-CoV-2; (b) Hydrogen bond with TYR458 residue,alkyl-alkyl interaction with PRO169, LEU172 residue of the protein and the complex.

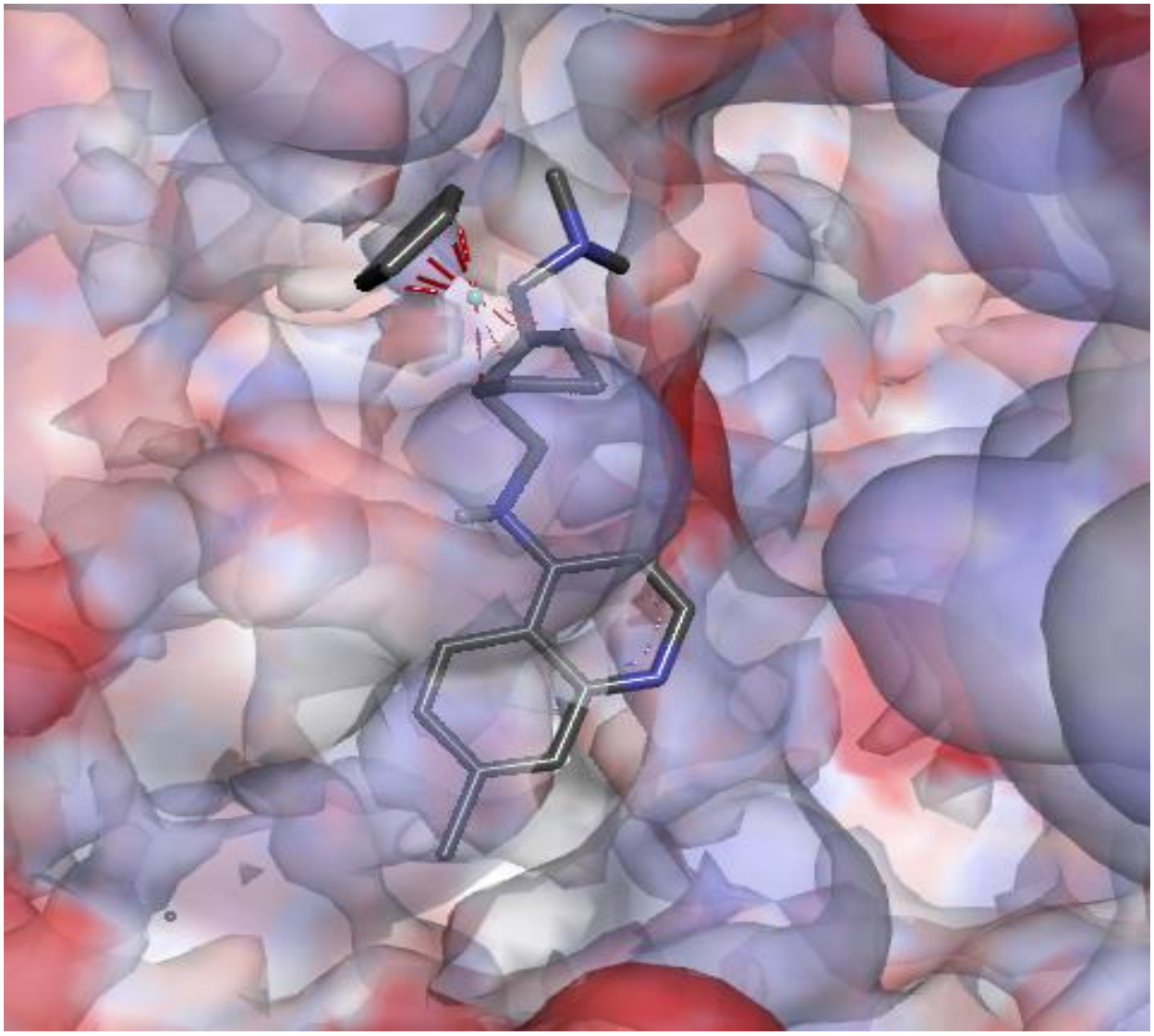

Figure S12. Docked pose of complex 5 in the RdRp complex of SARS-CoV-2.

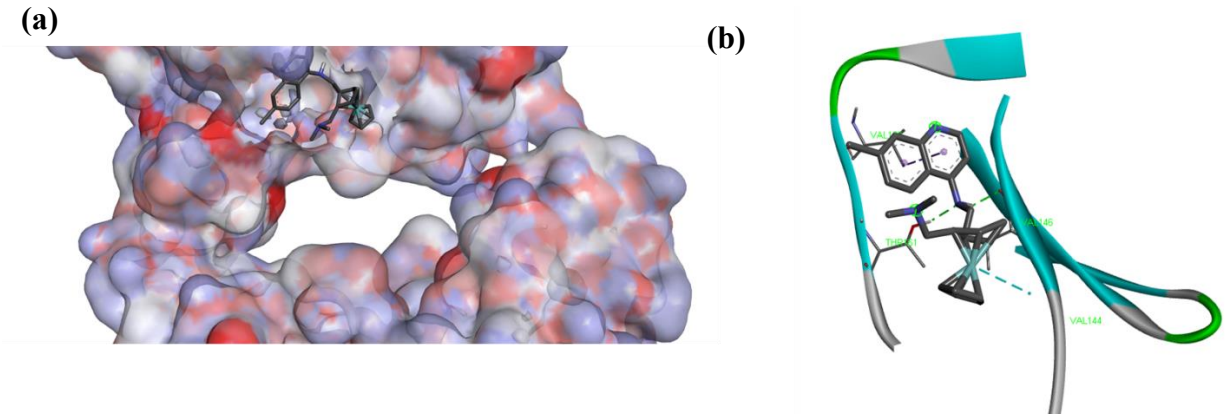

Figure S13. (a) Docked pose of complex 5 in the 4N0Y protein of HCV virus; (b Hydrogen bonding interactions with the VAL146 and THR 161 residue, alkyl-π interactions with the VAL159 residue of the protein 4N0Y and the complex.

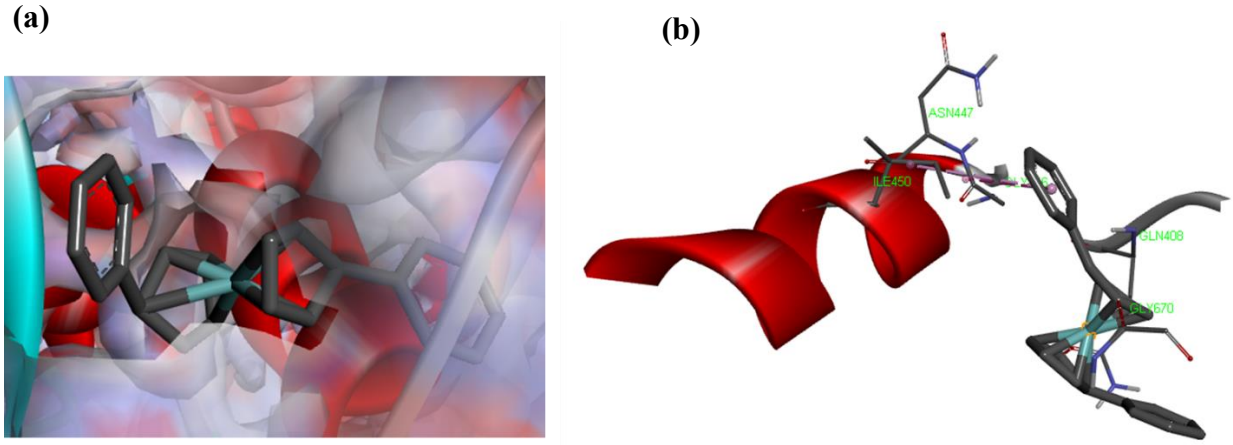

Figure S14. (a) Docked pose of control complex B in the RdRp of SARS-CoV-2; (b) Alkyl-π interactions with GLY446 and ILE 450 residue of protein and phenyl group of the complex.

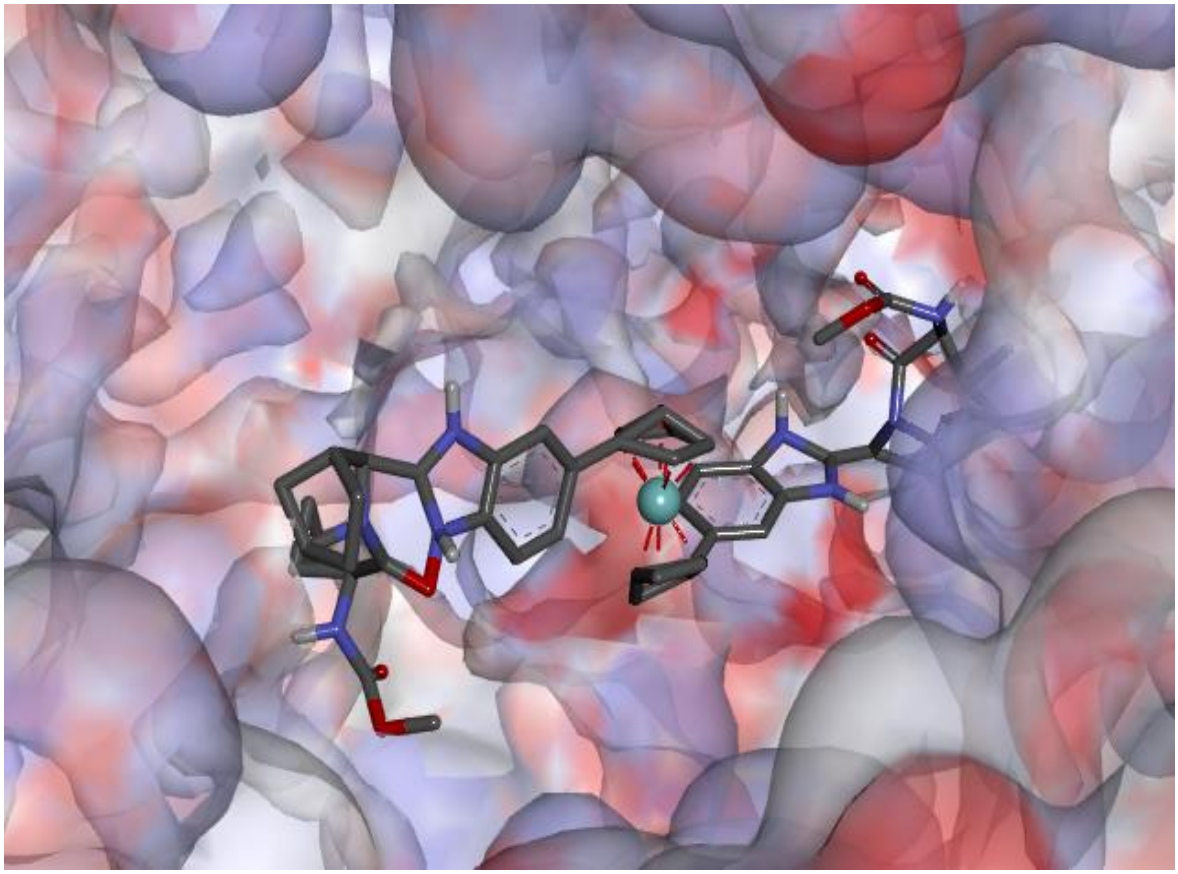

Figure S15. Docked pose of complex 6 in the RdRp complex of SARS-CoV-2.

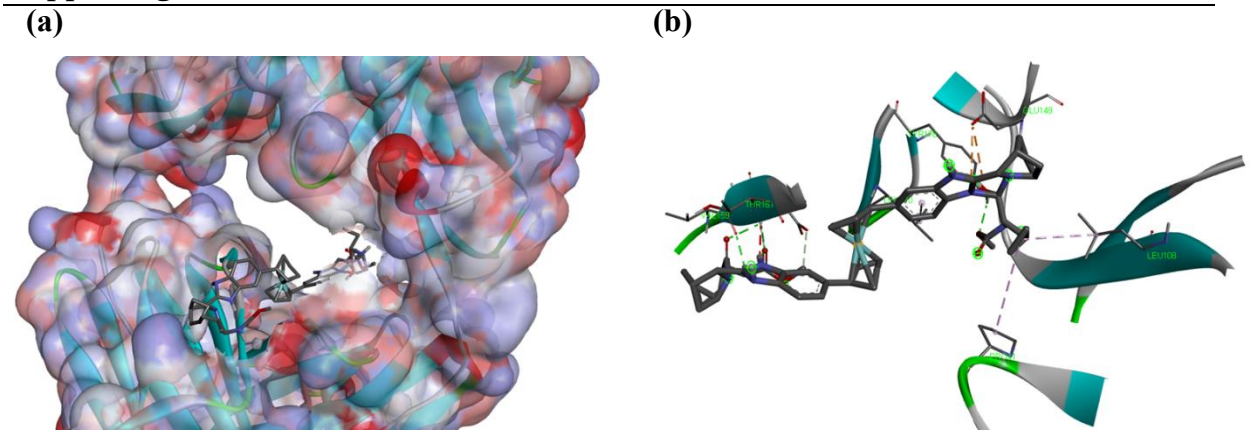

Figure S16. (a) Docked pose of complex 6 in the 4N0Y protein of HCV virus; (b) Hydrogen bonding interactions with the THR161, TYR176, VAL159 residue, alkyl-π interactions with the GLU160 residue of the protein 4N0Y and the complex.

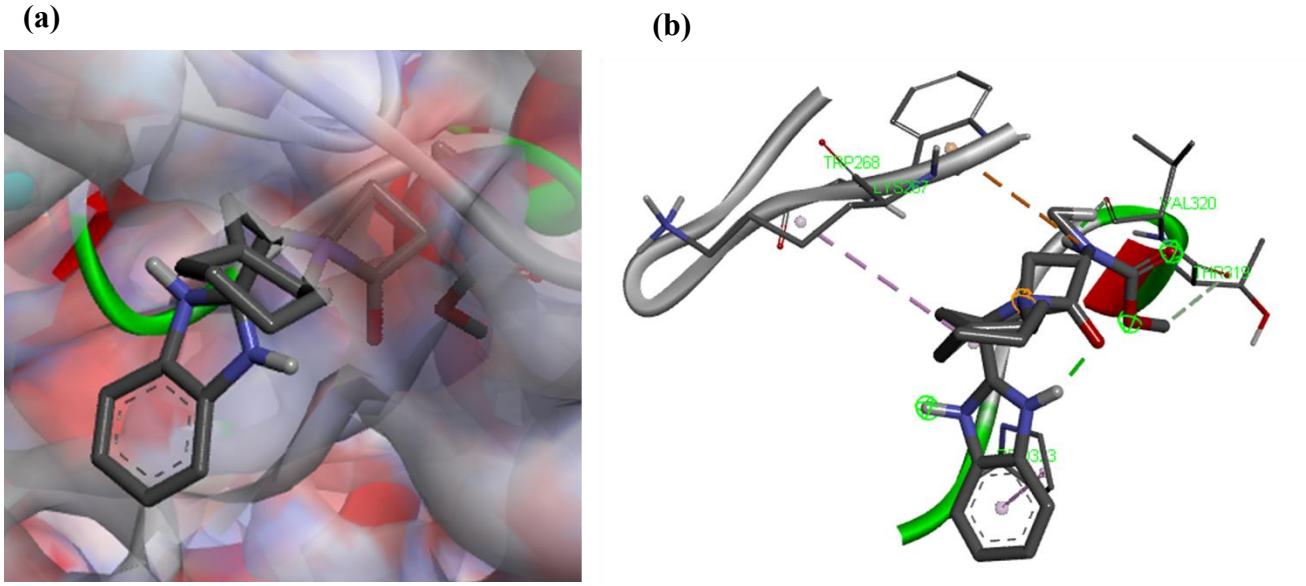

Figure S17. (a) Docked pose of quine in the RdRp of SARS-CoV-2; (b) Hydrogen bond interaction with the VAL320 residue of the protein and the ligand.

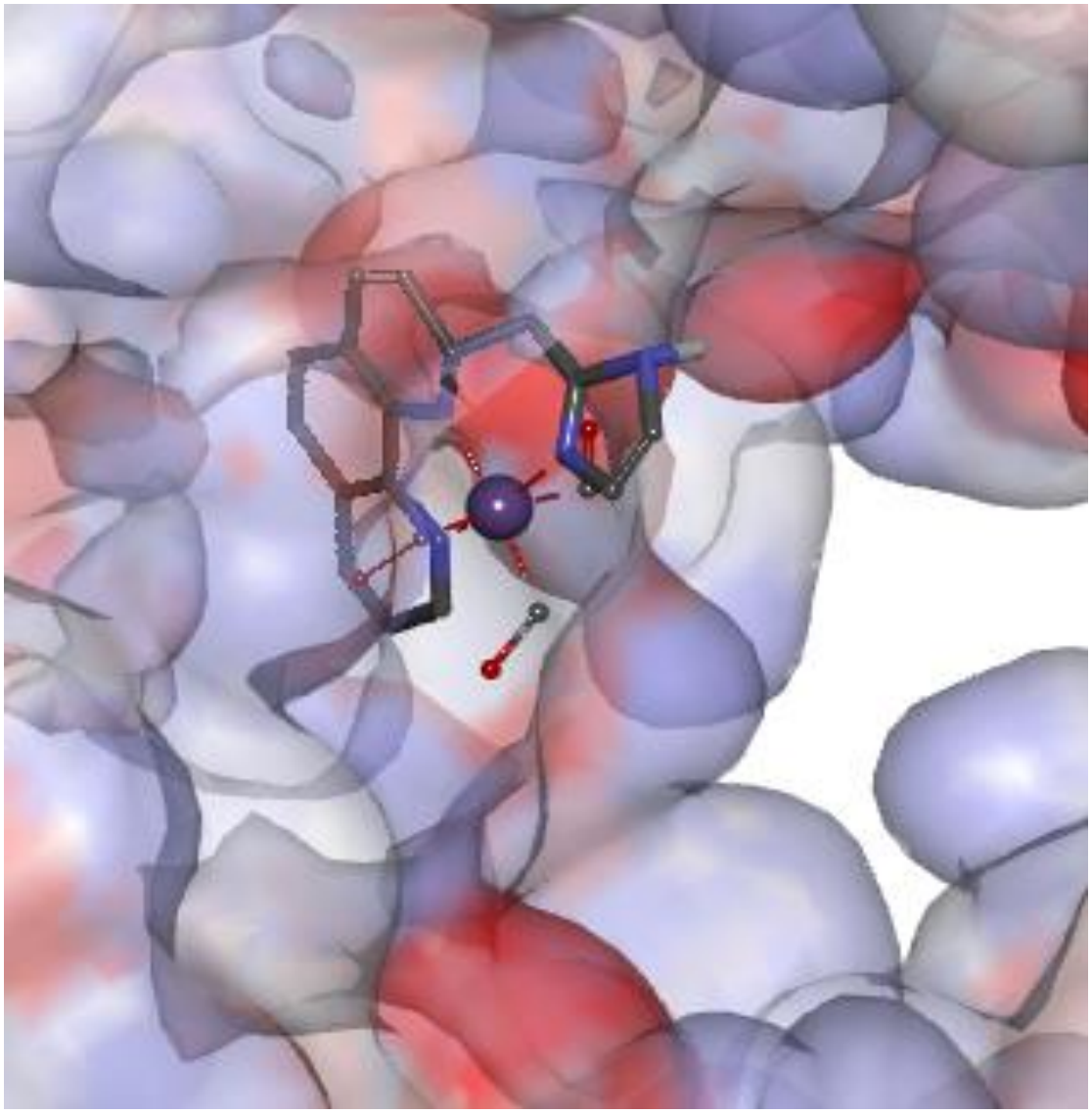

Figure S18. Docked pose of complex 7 in the RdRp complex of SARS-CoV-2.

(a) **(b)**

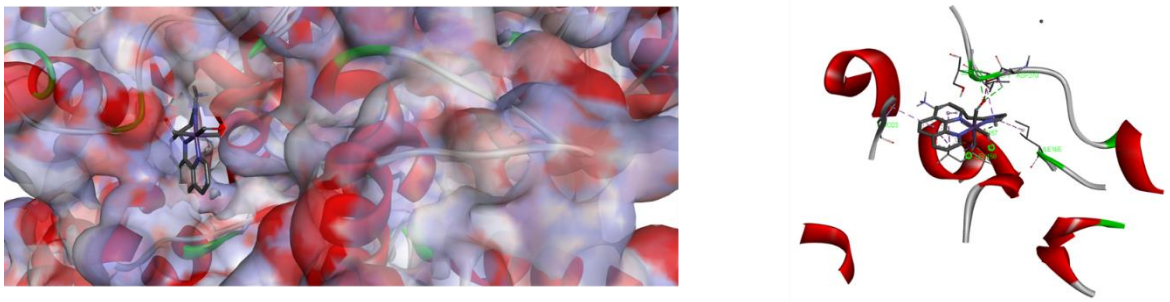

Figure S19. (a) Docked pose of complex 7 in the 5V13 protein of Mosquito juvinyle protein; (b) Hydrogen bonding interactions with the LYS157, LEU271, SER272 residue, alkyl-π interactions between ILE165, PRO23 residue of the protein 5V13 and the complex 7.

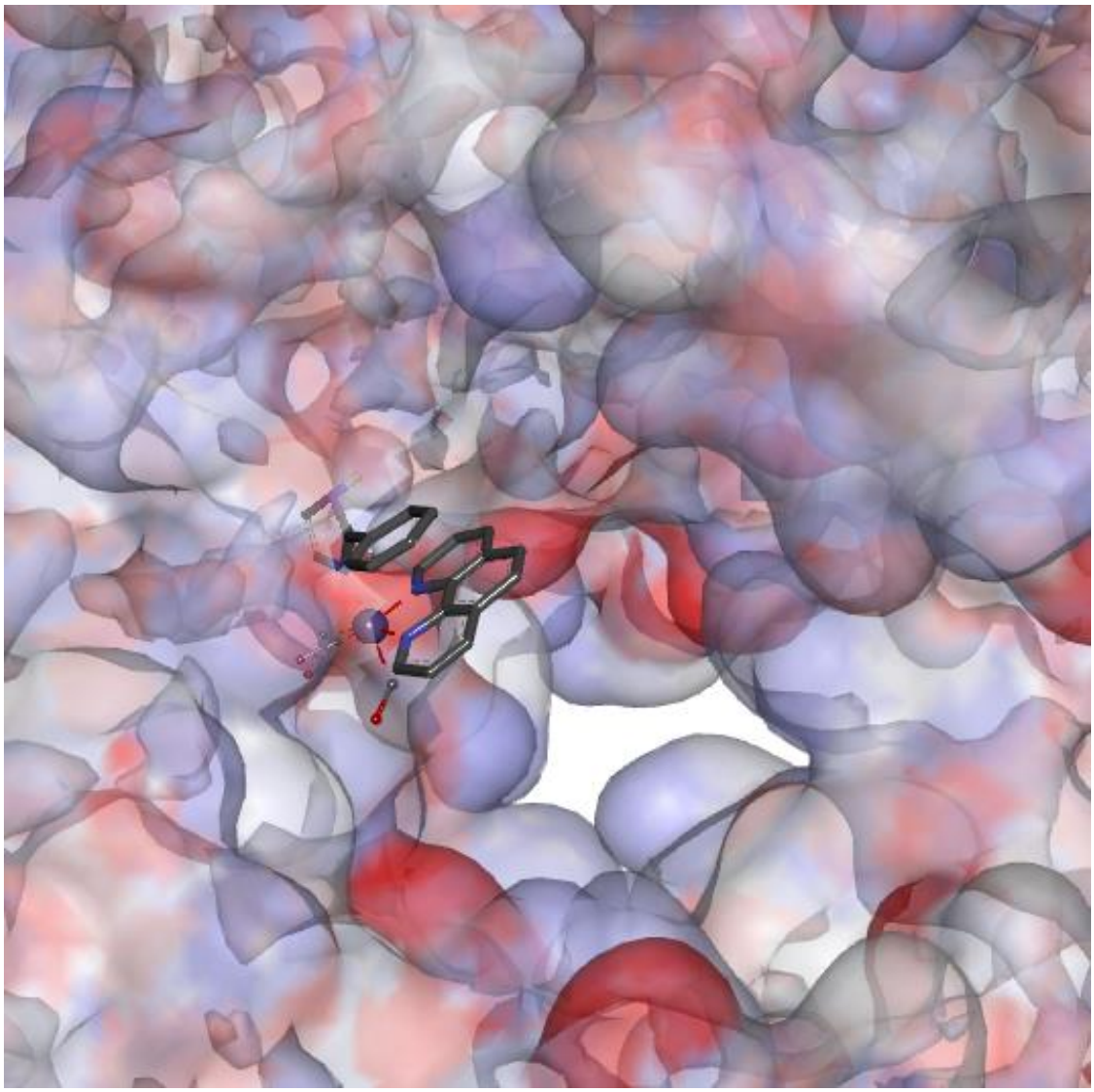

Figure S20. Docked pose of complex 8 in the RdRp complex of SARS-CoV-2.

(a) **(b)**

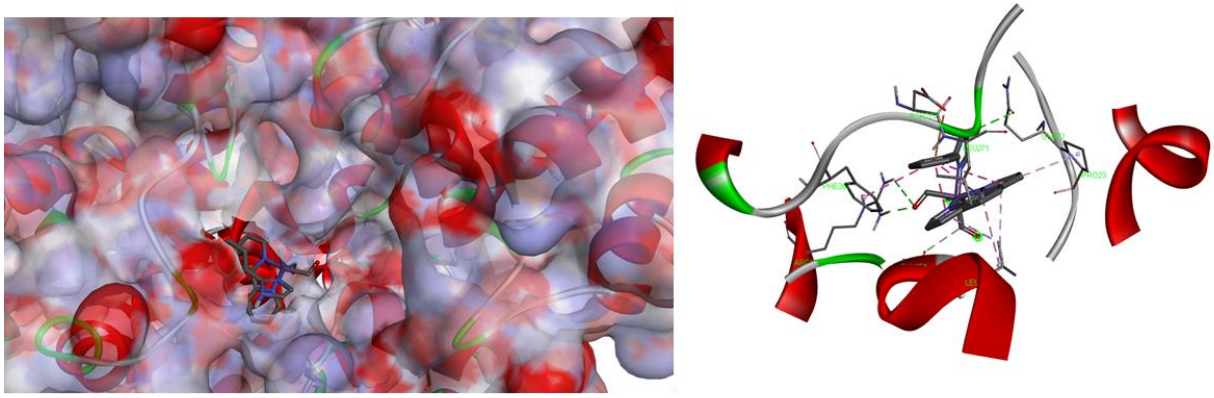

Figure S21. (a) Docked pose of complex 8 in the 5V13 protein of Mosquito juvinyle protein; (b) Hydrogen bonding interactions between the GLN22, ARG176 residue, alkyl-π interactions with the LEU358, LEU271, PRO23 residue of the protein 5V13 and the complex 8.

(a) **(b)**

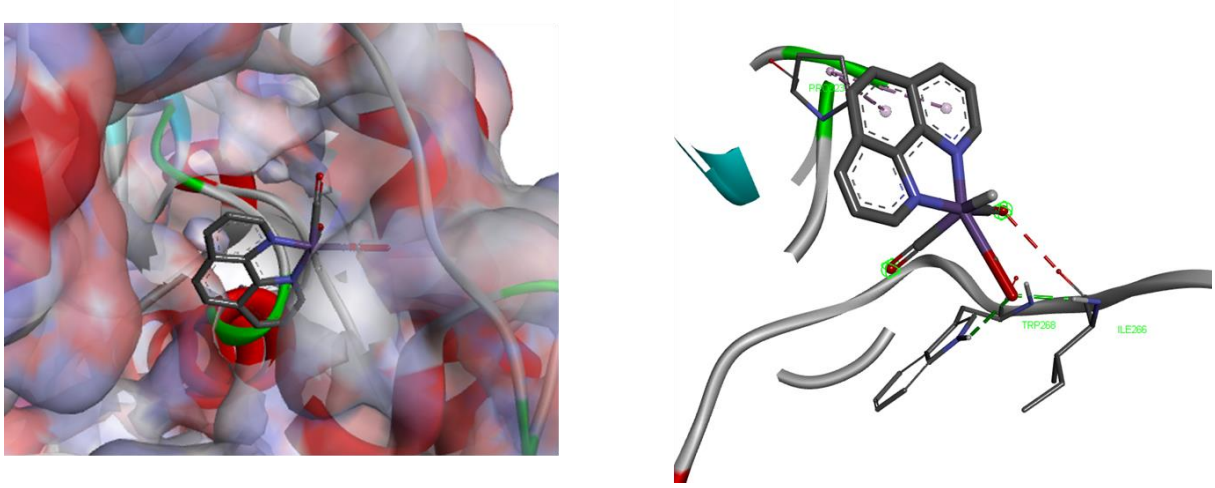

Figure S22. (a) Docked pose of control complex C in the RdRp of SARS-CoV-2; (b) Hydrogen bonding interactions with TYR256 and ILE266 residue of protein and carbonyl group of the complex.

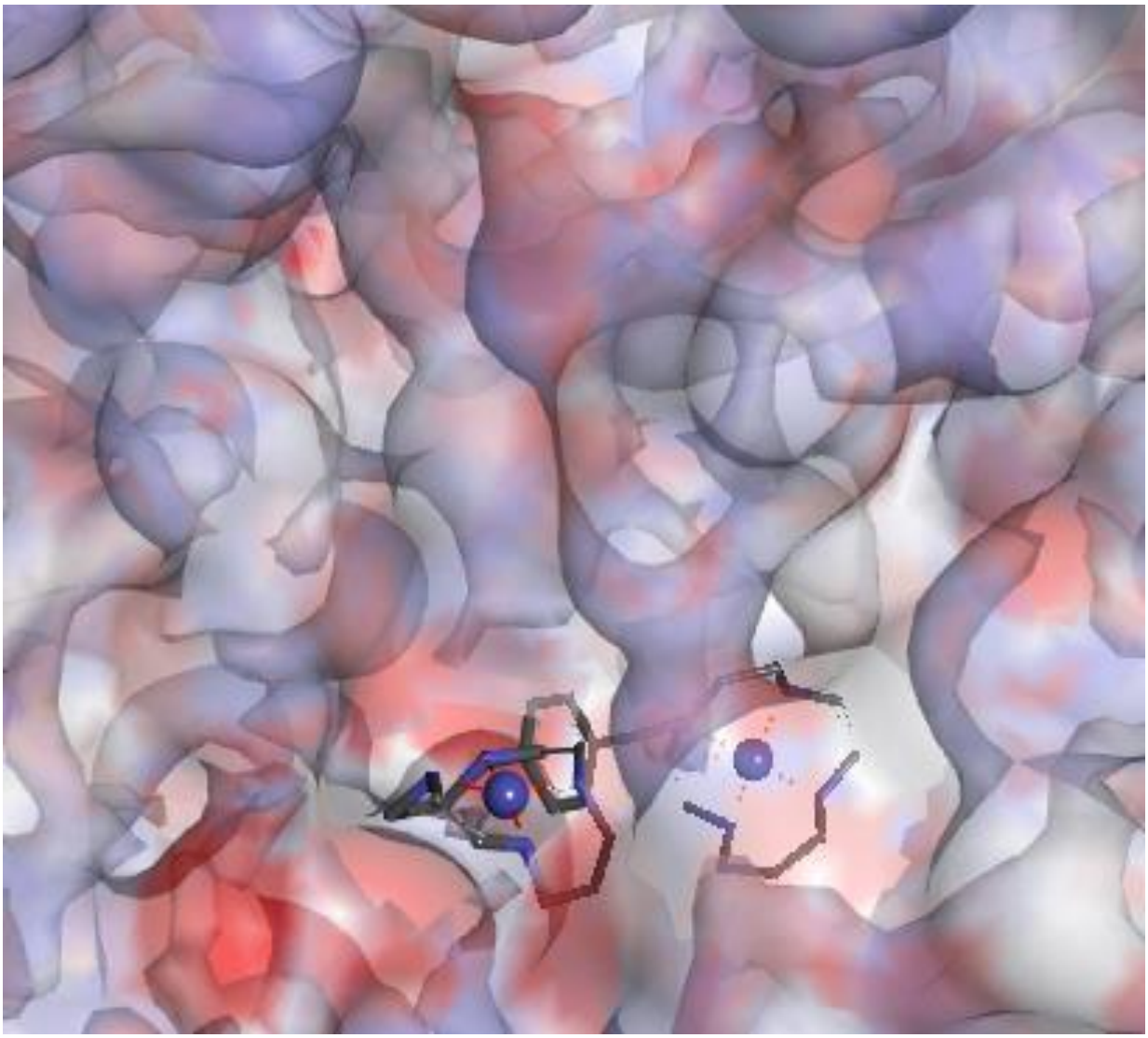

Figure S23. Docked pose of complex 9 in the RdRp complex of SARS-CoV-2.

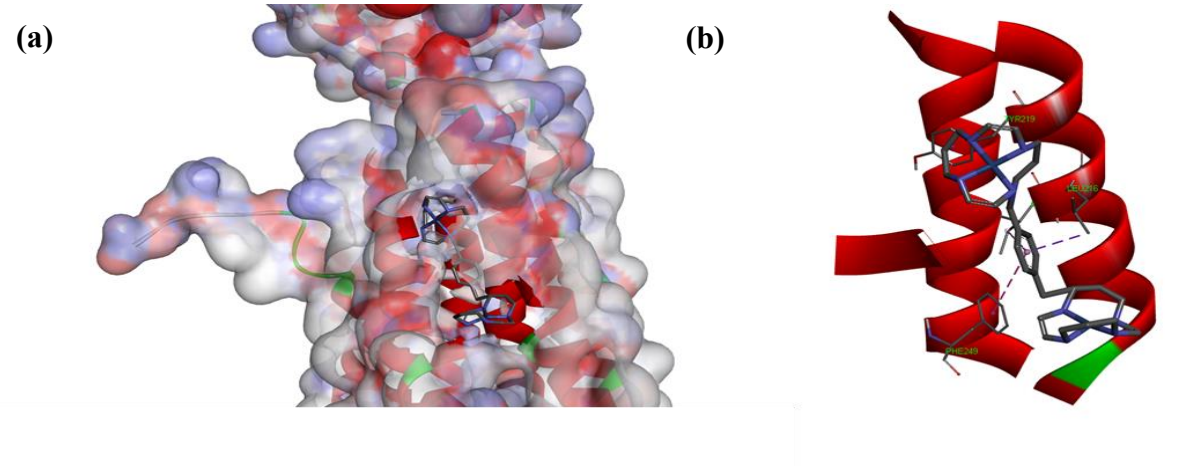

Figure S24. (a) Docked pose of complex 9 in the CXCR4 chemokine receptor (PDB ID 3OE6); (b) Alkyl-π interaction with the LEU216, PHE249, ILE215 residue, alkyl-alkyl interaction with TYR219 residue of the protein and the complex.

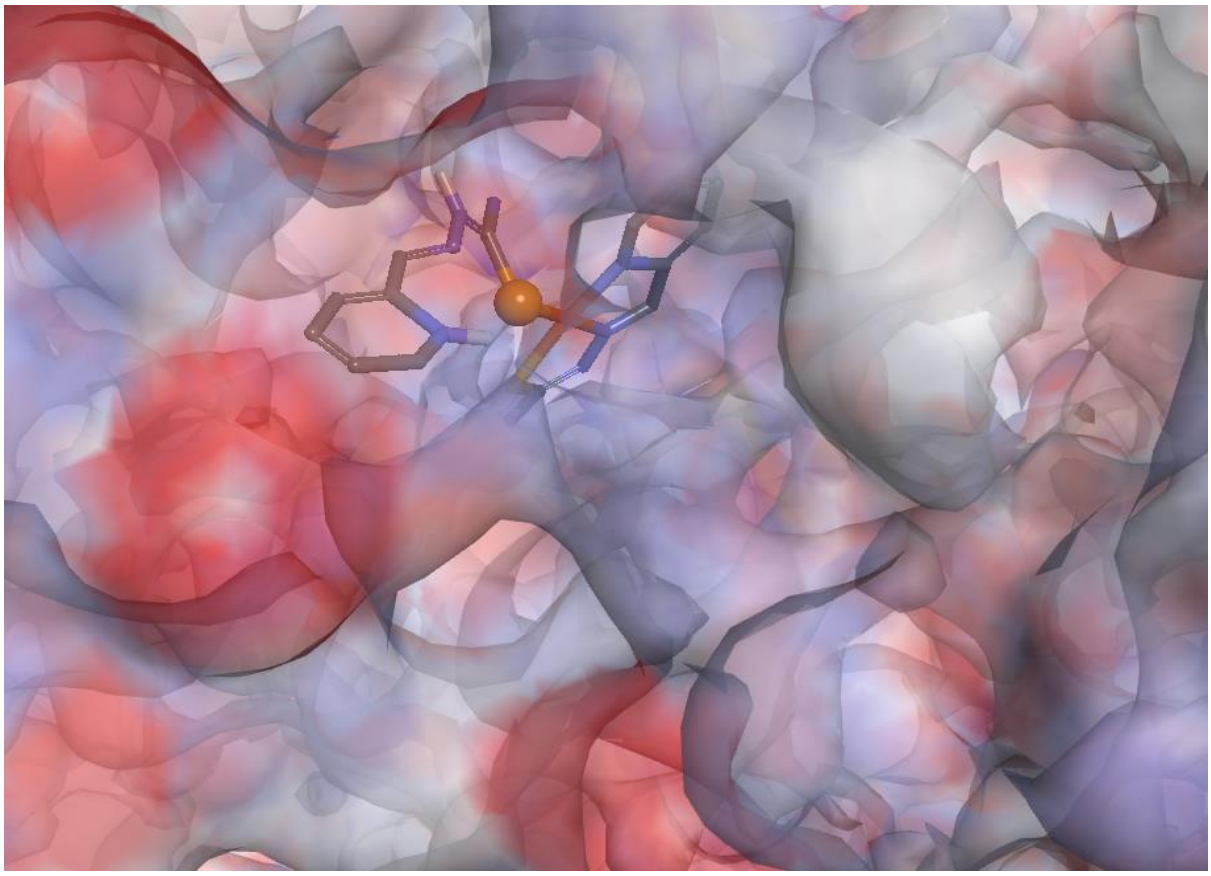

Figure S25. Docked pose of complex 10 in the RdRp complex of SARS-CoV-2.

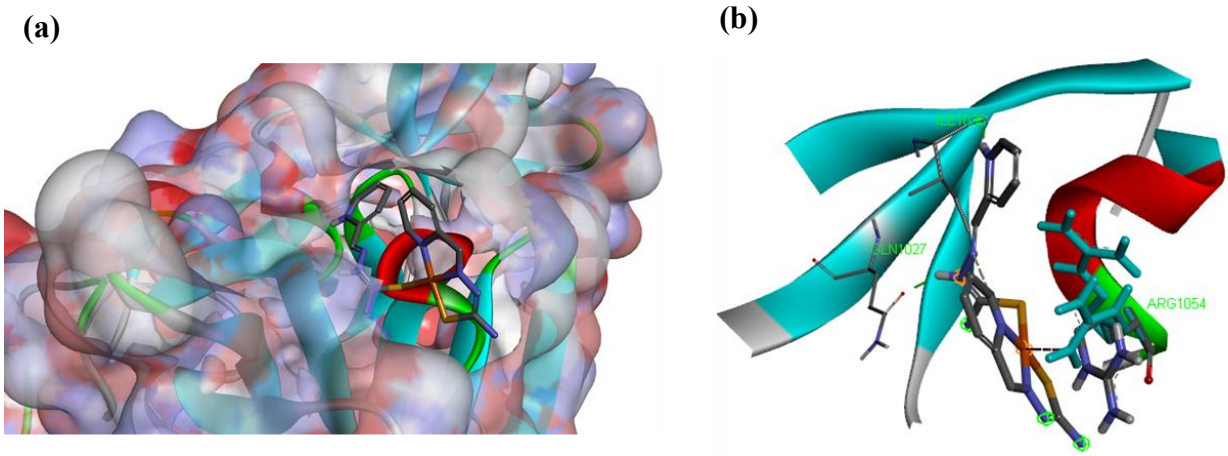

Figure S26. (a) Docked pose of complex 10 in the Dengue virus protease (PDB ID 4M9F); (b) Hydrogen bonding interactions with the ILE1036 and GLN1027 residue, coordinate covalent bond with Pt and ARG1054 residue of the protein and the complex.

(a) **(b)**

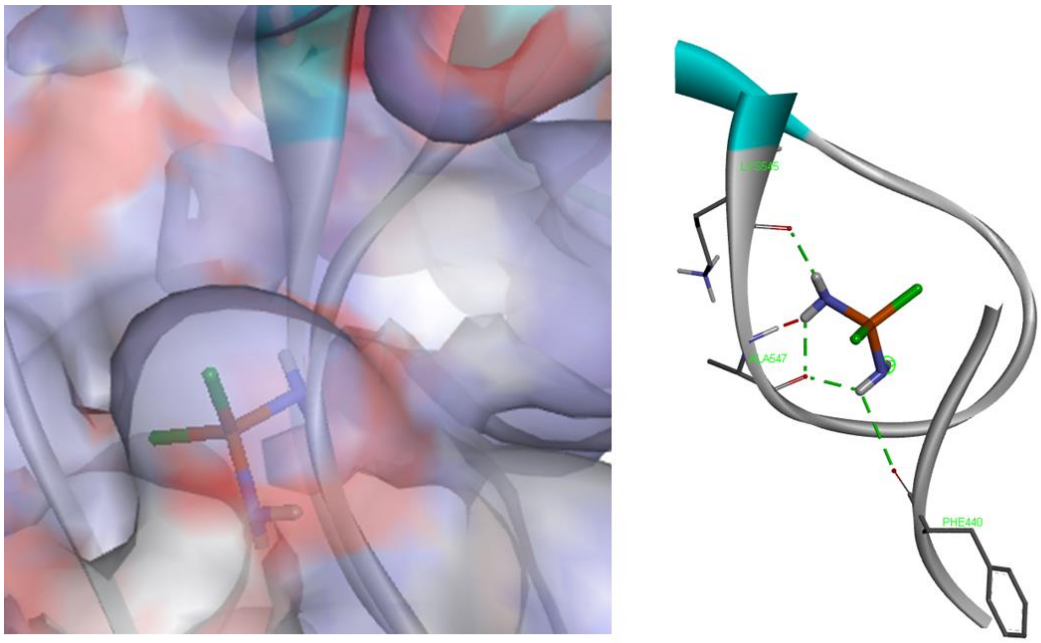

Figure S27. (a) Docked pose of control complex D in the RdRp of SARS-CoV-2; (b) Hydrogen bonding with LYS545, ALA547 and PHE440 residue of the protein with the complex.

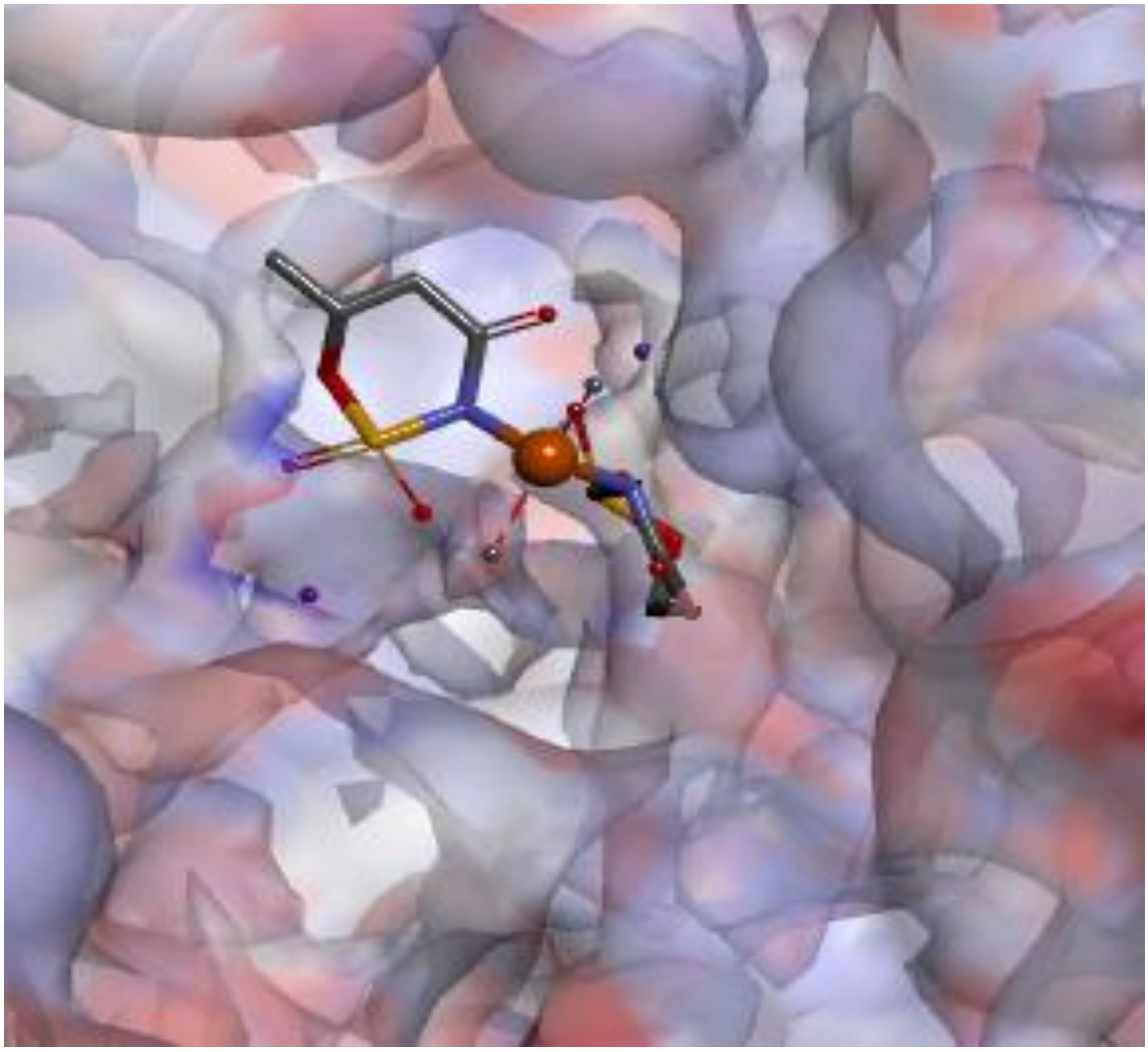

Figure S28. Docked pose of complex 11 in the RdRp complex of SARS-CoV-2.

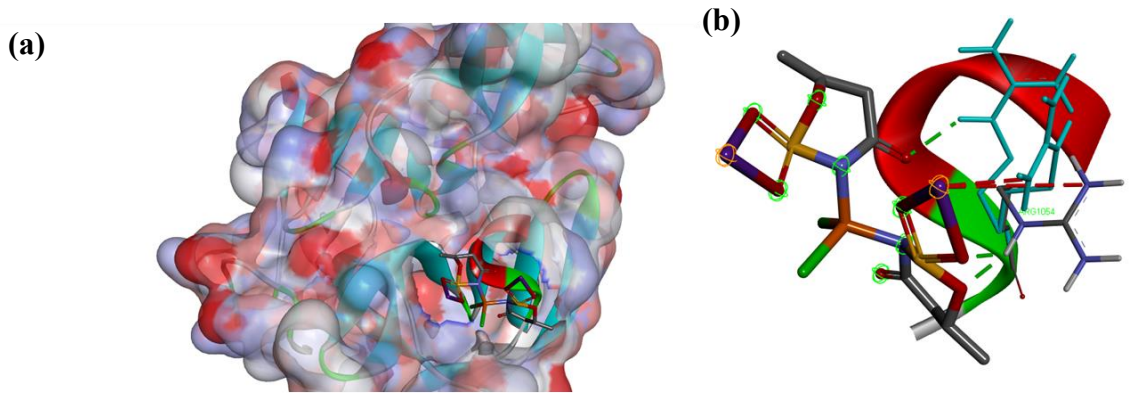

Figure S29. (a) Docked pose of complex 11 in the Dengue virus protease 4M9F; (b) Hydrogen bonding interactions with the ILE1036 and ARG1054 residue of the protein with the complex.

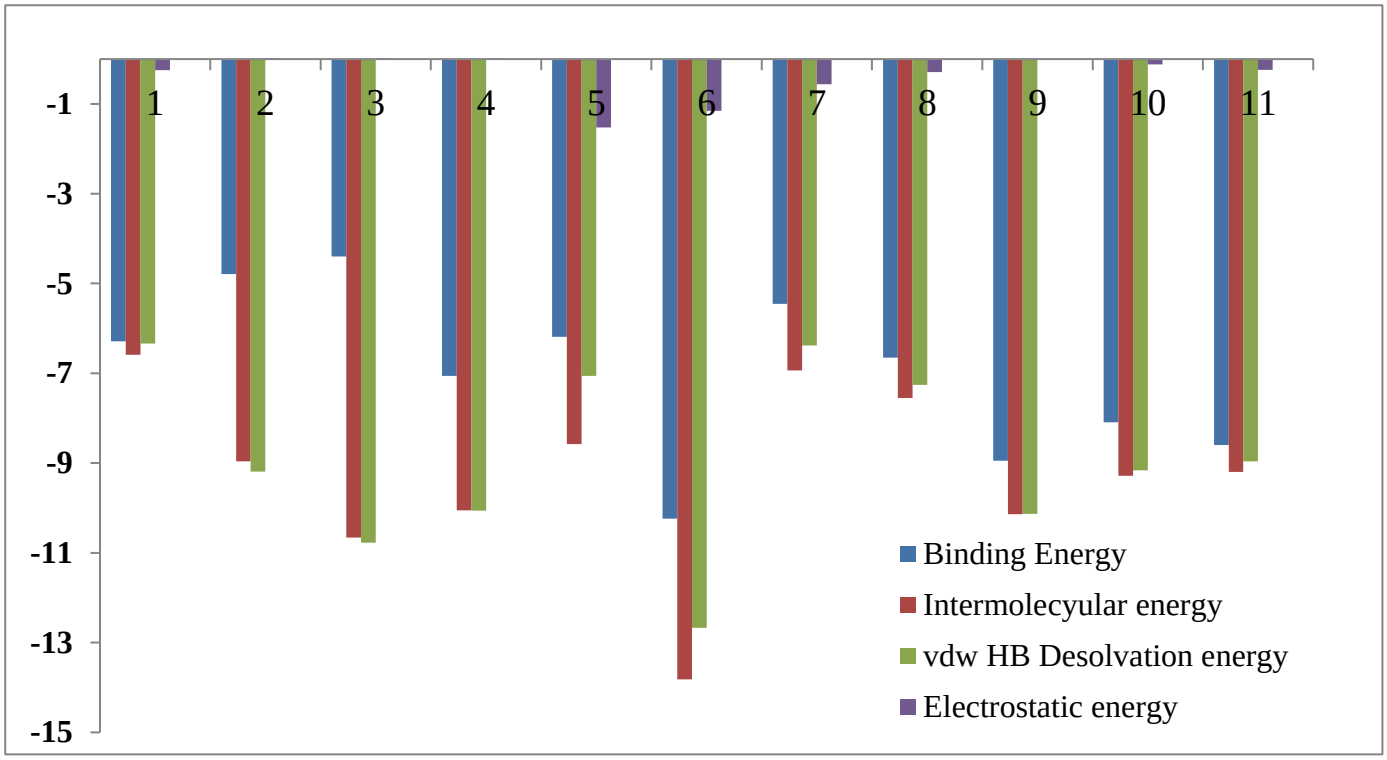

Figure S30. Docking interaction comparative data

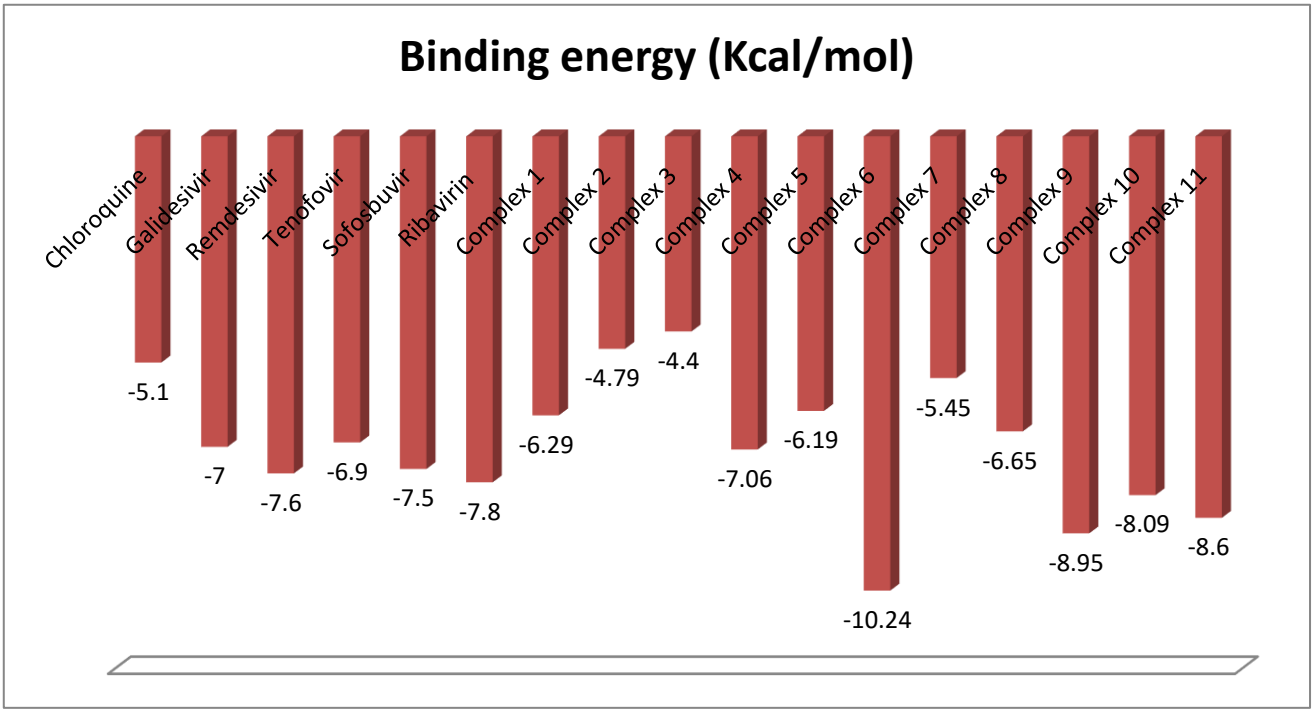

Figure S31. Binding energies between compounds and RdRp of SARS-CoV-2 comparative data

References

1. M. Gil-Moles, U. Basu, R. Büssing, H. Hoffmeister, S. Türck, A. Varchmin, I. Ott, *ChemRxiv. Preprint*., 2020, DOI: 10.26434/chemrxiv.12488390.v1
2. D. A. Milenkovic, D. S. Dimic, E. H. Avdovic, and Z. S. Markovic, RSC Adv., 2020, 10, 35099.